Nanoscale

Accepted Manuscript

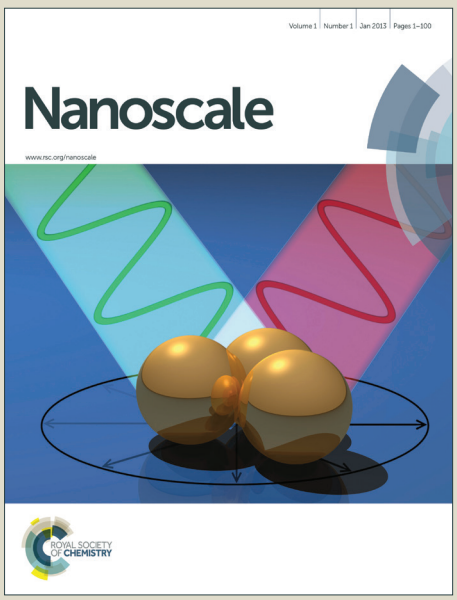

ROYAL SOCIETY OF CHEMISTRY

www.rsc.org/nanoscale

Journal Name

RSCPublishing

Cite this: DOI: 10.1039/x0xx00000x

The Use of pH-sensitive Functional Selenium Nanoparticles Shows Enhanced *in vivo* VEGF-siRNA Silencing and Fluorescence Imaging

Qianqian Yu,[a,1] Yanan Liu,[a,b,1] Chengwen Cao,[a] Fangling Le,[a] Xiuying Qin,[a] Dongdong Sun,[a] and Jie Liu. [a,*]

Received 00th January 2014,
Accepted 00th January 2014

DOI: 10.1039/x0xx00000x

www.rsc.org/

The utility of small interfering RNAs (siRNAs) has shown great promise in treating a variety of diseases including many types of cancer. While their ability to silence a wide range of target genes underlies their effectiveness, therapies application remain hindered by a lack of an effective delivery system. In this study, we sought to develop an siRNA-delivery system for VEGF, a known signaling molecule involved in cancer, that consists of two selenium nanoparticles SeNPs and G2/PAH-Cit/SeNPs. G2/PAH-Cit/SeNPs is a pH-sensitive delivery system that is capable of enhancing siRNA loading, thus increasing siRNA release efficiency and subsequent target gene silencing both *in vitro* and *in vivo*. *In vivo* experiments using G2/PAH-Cit/SeNPs@siRNA led to significantly higher accumulation of siRNA within the tumor itself, VEGF gene silencing, and reduced angiogenesis in the tumor. Furthermore, the G2/PAH-Cit/SeNPs delivery system not only enhanced anti-tumor effects on tumor-bearing nude mice as compared to SeNPs@siRNA, but also resulted in weak occurrence of lesions in major target organs. In sum, this study provides a new class of siRNA delivery system, thereby providing an alternative therapeutic route for cancer treatment.

Introduction

RNA interference (RNAi) is a powerful tool designed to silence specific genes, lending itself well to genetic therapy applications.[1,2] The process utilizes small interfering RNA (siRNA) to induce the sequence-specific degradation of homologous messenger RNA (mRNA), thereby resulting in the suppression of protein expression.[3-5] Therefore, siRNA can be utilized for silencing a wide range of target genes to treat a variety of diseases, including cancers.[6-8]

Angiogenesis, progress and satisfy the proliferating tumor cells for nutrients and oxygen.[9] Inhibition of vascular endothelial growth factor (VEGF) which plays a significant role in angiogenesis has become a new way to suppress tumor growth and metastasis.[10,11] Therefore, RNAi-mediated silencing of VEGF expression has become a focus of cancer research and has been shown to successfully inhibit the expression of VEGF resulting in stopped the proliferation of vascular endotheliocyte and angiogenesis.[12, 13] However, the therapeutic application of any type of siRNA requires the development of an effective delivery vehicle. With this in mind, one of the biggest challenges is to find an ideal gene delivery system which fulfills three criteria: that it has prolonged circulation in the blood stream, enhanced accumulation in

the target tissue, and that it allows intact siRNA to be efficiently transported intracellularly.[14-16]

Dendrimers as siRNA delivery systems, have been largely explored especially for the treatment of cancer.[17, 18] However, Cationic poly(amidoamine) (PAMAM) dendrimers possess relatively high gene transfection efficacy with serious cytotoxicity to transfected cells.[19] To achieve higher gene transfection efficacy, PAMAM dendrimers were functionalized with hydrophobic chains, including aliphatic acid [20] and amino acids [21] along with targeting moieties such as folic acid [22] and lactose.[13] Additionally, nanoparticles such as gold nanoparticles [23] have also been used to increase transfection efficiency. Moreover, selenium nanoparticles (SeNPs) have attracted increasing attention due to their excellent anti-cancer potential and concomitant low cytotoxicity.[24] Recently, we reported functionalized selenium nanoparticles having both a greater tumor-targeting efficacy and resulting inhibition of tumor growth and vascularization.[25, 26]

Based on this past research, we sought to use siRNA to suppress the VEGF gene in order to inhibit tumor growth and metastasis in cancer. To do this, we developed two nanoparticle delivery systems, selenium nanoparticles (SeNPs) and G2/PAH-Cit/SeNPs, additionally, poly (allylamine hydrochloride)-citraconic anhydride (PAH-Cit) can be readily converted back to cationic poly (allylamine) through amide hydrolysis upon exposure to an acidic environment like that found within late endosomes and lysosomes.[27] We thus embedded PAH-cit into generation 2 PAMAM (G2)-based SeNPs to facilitate the load and release of siRNA in a cellular environment. The strategy of constructing G2/PAH-Cit/SeNPs delivery system is illustrated in Scheme 1.

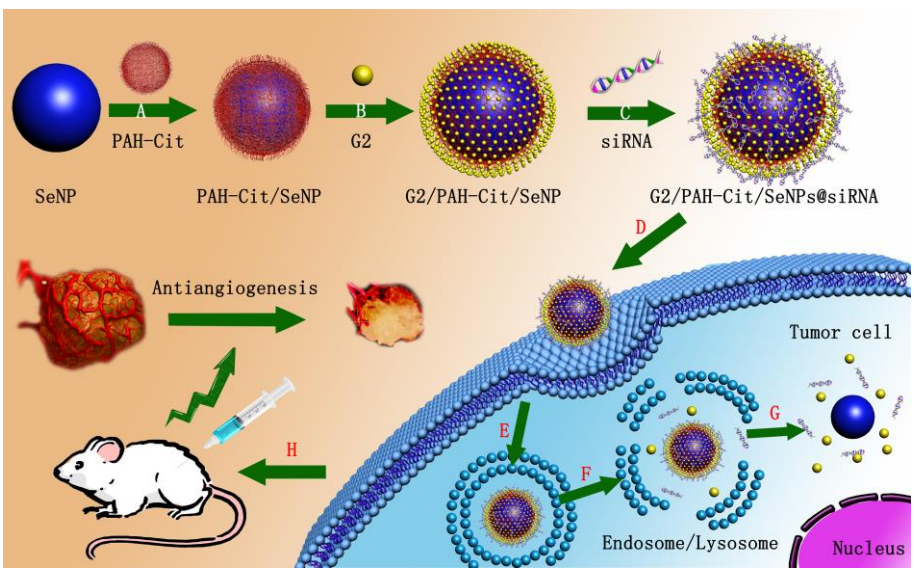

Scheme 1. Flowchart illustrating the preparation of siRNA delivery bectors G2/PAH-Cit/SeNP@siRNA based on selenium nanoparticles (SeNPs) and gene silencing process.

Materials and methods

Materials and reagents

All reagents and solvents were purchased commercially and used without further purification unless specially

noted, and Ultrapure MilliQ water (18.2 MW) was used in all experiments. Na_2SeO_3, PAH (15 kDa), Citraconic anhydride (Cit) and G2 (molecular weight 3252 Da) and G5 (molecular weight 28826 Da) PAMAM dendrimers were purchased from Sigma-Aldrich Chemical Co. PAH-Cit was synthesized according to the reported procedure.[28] VEGF siRNA and enhanced greenfluorescent protein siRNA (EGFP) were purchased from Bioneer Co. (Daejeon, Korea). and the sequences were as follows: sense strand, 5'-AUGUGAAUGCAGACCAAAGAATT-3'; antisense strand antisense strand, 3'-TTUAACACUUACGUCUGGUUU-CUU-5'. The siRNA was labeled with FITC at the 5'-end of its sense strand. Fetal bovine serum (FBS) was purchased from Gibco (Life Technologies AG, Switzerland). 3-(4, 5-dimethylthiazol-2-yl)-2, 5-diphenyltetrazolium bromide (MTT), 4'6-diamidino-2-phenylindole (DAPI), LysoTracker Red, and Hoechst 33342 were from Sigma (St. Louis, MO, U.S.).

Preparation of SeNPs and G2/PAH-Cit/SeNPs loaded with/without siRNA

SeNPs was prepared as previously reported [29] with minor modifications. The SeNPs was synthesis as follow: 0.2 mL aliquot of Na_2SeO_3 stock solution was heated to 40 ℃, then 4.8 mL of fresh Cys solution (25 mM) was drop wise added, and the mixture was reconstituted to a final volume of 10 mL with Milli-Q water. Purification of the crude SeNPs was performed twice at 15 200 *g* for 20 min, and the SeNPs were resuspended in 10 mM HEPES buffer (pH=7.4). Charge-reversal G2/PAH-Cit/SeNPs were prepared with G2 PAMAM, charge-reversal PAH-Cit, and SeNPs by layer-by-layer assembly technique.[30] For Both deposition steps, PAH-Cit/SeNPs and G2/PAH-Cit/SeNPs, each coating step was performed for 30 min after the addition of the selenium nanoparticles to the respective stirring solution. After G2 coating, G2/PAH-Cit/SeNPs was collected twice at 5000 *g*/min for 10 min and resuspended in 10 mM HEPES buffer. To load siRNA onto the prepared vehicles, 1 μg/μL of siRNA solution in 10 mM sterile HEPES buffer was combined with SeNPs or G2/PAH-Cit/SeNPs at various N/P ratios to siRNA. N here represents the number of surface amine groups of the dendrimers, P represents the number of phosphate anions in the DNA chains. The resulting mixtures were mixed by pipetting and incubated at room temperature for 30 min before use.

Characterization of SeNPs and G2/PAH-Cit/SeNPs

The as-prepared products were characterized by using various methods. Transmission electron microscopy (TEM) samples were prepared by dispersing the nanoparticles solution onto a holey carbon film on copper g rids. The micrographs were obtained on Hitachi (H-7650) for TEM operated at an accelerating voltage at 80 kV. The zeta potential and size distribution of the nanoparticles was measured by PCS on a Nano-ZS instrument (Malvern Instruments Limited). SEM-EDX analysis was carried out on an EX-250 system (Horiba) and employed to examine the elemental composition of SeNPs and G2/PAH-Cit/SeNPs (Fig.S1).

A garose gel electrophoresis assay

7.5 μL of delivery systems at various N/P ratios from 0.5 : 1 to 8.0 : 1 in pH 7.4 HEPES buffer and 2.5 μL of 80% glycerol were mixed and subjected to 2 % agarose gel electrophoresis containing 0.5 μg/mL ethidium bromide per well. Electrophoresis was carried out at a voltage of 80

V for 20 min in TBE running buffer. To evaluate the protection of siRNA by delivery systems, 2 μL of RNaseA (5 U/μL) was used to digest 0.5 μg of siRNA formulated with delivery systems at 37 ℃ for 1 h. After digestion, 5 μL of 2 % SDS was added to dissociate siRNA from delivery systems. Images were recorded by Image Quant 300 (GE Healthcare, America).

siRNA loading and release from the delivery systems

The loading capacity of siRNA, 10 μg of siRNA was mixed with varying N/P ratio (1.0 : 1, 5.0 : 1, 10.0 : 1) of SeNPs or G2/PAH-Cit/SeNPs for different times (10 min, 30 min, and 1 h) at room temperature. For the loading quantity assay, SeNPs@siRNA or G2/PAH-Cit/SeNPs@siRNA were centrifuged at 5 000 *g* at 4℃, and the supernatant was collected and the siRNA quantity was assessed by using a Perkin- Elmer Lambda – 850 (PerkinElmer, USA) at an absorbance of 210 nm. Subtraction of the quantity from the initial amount of siRNA resulted in the loaded amount of siRNA onto the nanoparticles. The release profile of siRNA, SeNPs or G2/PAH-Cit/SeNPs was complexed with siRNA at N/P ratio of 5.0:1 in 10 mM HEPES buffer at either pH 5.5 or 7.4 and incubated in a 96-well culture plate at 37℃. Samples were taken from the plate at scheduled time points and centrifuged at 5000 g for 10 min, and the concentration of siRNA in 1 μL of supernatant was measured using an fluorescence spectra (e-spect, Malcom, Japan).

Cell lines and cultures

Several human cell lines used in this study, including HeLa, A549, HepG2, HUVEC and NIH/3T3 cells were purchased from American Type Culture Collection (ATCC, Manassas, VA). All cell lines were maintained in either RPMI-1640 or DMEM media supplemented with penicillin (100 units/mL), fetal bovine serum (10%), and streptomycin (50 units/mL) at 37℃ in a humidified 5% CO_2 atmosphere.

Cell viability

The cytotoxicity of delivery systems was determined through using transform thiazolyl blue tetrazolium bromide (MTT) assay.[31] Briefly, cells were seeded in 96-well plates at a density of 4×10^3 cells/well for 24 h. The cells were incubated at different concentrations of delivery systems for various periods of time. After treatment, 20 mL of MTT solution (5 mg/mL in PBS) was added to each well and incubated for 4 h, and then the medium was removed and 200 mL DMSO was added to dissolve the formazan crystals.

***In vitro* gene transfection**

A549 and HUVEC cells were cultured in 24-well plates for 24 h before *in vitro* gene transfection. Generally, 2.0 μg enhanced green fluorescent protein (EGFP) plasmids were mixed with different delivery systems at N/P ratios of 5 : 1, 10 : 1 and 20 : 1 for 30 min before adding into the plates. After incubation for 6 h, 500 μL fresh DMEM medium with 10 % serum was added to each well of the plates. For EGFP gene transfection, EGFP expression after 48 h was observed by a fluorescent microscopy (Olympus, Japan) or a Leica TCS SP5 confocal microscope (Leica Microsystems, Wetzlar, Germany).

Flow cytometric analysis

Cellular uptake was detected with the fluorescent intensity of FITC - siRNA in the cells. The A549 or HUVEC cells were cultured in 24-well plates overnight and 0.5 μg/mL siRNA, 5 μg/mL SeNPs@siRNA or G2/PAH-Cit/SeNPs@siRNA were added. After 6 h of incubation, the cells were collected, and washed with PBS buffer, cells were analyzed using a FACS Calibur (BD FACSAria).

ICP-AES analysis

Se concentration of the cells was determined by the ICP-AES method. Briefly, the sample was digested with 3 mL of concentrated nitric acid and 1 mL of H_2O_2 in a digestive stove (Qian Jian Measuring Instrument Co., Ltd., China) at 180 ℃ for 3 h. The digested product was reconstituted to 10 mL with Milli-Q H_2O and used for ICP-AES analysis.

Live cell confocal microscopy

HepG2 and HUVEC cells were were seeded in a laser confocal microscopy 35 mm^2 Petri dish (MatTek, USA) to 70 % confluence. Delivery system labeded with FITC-siRNA was prepared in serum media and incubated for 15 min at room temperature. After transfect delivery system in cells for varying amounts of time at 37 ℃ and the cells were washed 3 times with 1×PBS and lysosome staining was performed by 500 nM LysoTracker Red for 15 min. The cells were then washed with PBS (2×200 μL) and photographed with a Leica TCS SP5 confocal microscope (Leica Microsystems, Wetzlar, Germany) using a planapochromate 63×/NA 1.4 oil immersion objective. The fluorescence signal of FITC-siRNA was detected at 520～560 nm with an excitation at 488 nm and LysoTracker Red signal was obtained at 580～650 nm with an excitation at 577 nm.

Internalization of G2/PAH-Cit/SeNPs@siRNA by TEM imaging

For TEM, cells were incubated with G2/PAH-Cit/SeNPs@siRNA (5 μg/mL, 1 h, 6 h and 24 h) then fixed using 3 % glutaraldehyde and dehydrated using ethanol. TEM samples were sectioned in Araldite resin by microtome and examined on a FEI Tecnai instrument operating at 80 kV equipped with a Gatan 1 k CCD Camera.

Western blot analysis

HUVEC cells with delivery systems treatment for 48 h were incubated with lysis buffer (Beyotime) to obtain total cellular proteins. The protein concentration was examined by BCA assay. Equal amount of proteins were eletrophoresed in 12% tricine gels and then transferred to nitrocellulose membrane and blocked with 5% non-fat milk in Tris-Buffered Saline Tween-20 (TBST) buffer for 1 h. Then the membranes were incubated with primary antibodies at 1:1000 dilution in 5 % non-fat milk overnight at 4 ℃ with continuous agitation. Then the membranes were incubated with secondary antibodies conjugated with horseradish peroxidase at 1 : 2000 dilution for 1 h at room temperature, followed by 3 times washing with TBST. The bands were then visualized using horseradish peroxidase-conjugated secondary antibodies (1 : 2000) followed by ECL (Pierce Biotech, Rockford, IL). β-Actin was used to confirm the comparable amount of proteins in each lane.

Tube formation assay

Matrigel was dissolved at 4 ℃ for overnight, and each well of prechilled 24-well plates was coated with 100 μL Matrigel and incubated at 37 ℃ for 45 min. HUVECs (4×10^4) were added in 1 mL endothelial cell growth medium with various concentration of complexes. After 24 h of incubation at 37 ℃, 5 % CO_2, endothelial cell tube formation was assessed with an inverted photo-microscope. Tubular structures were quantified by manual counting of low-power fields and percent inhibition was expressed using untreated wells as 100 %.

Invasion assay

The invasion assay was performed in Transwell (8 mm pore; Corning, Lowell, MA) pre-coated with matrigel for 8 h at 37 °C. The bottom chambers were filled with 600 mL DMEM/F12 with 1 % FBS supplemented with VEGF (20 ng/mL). HUVECs (5 ± 10^4 cells per chamber) suspended in 100 mL DMEM/F12 with 1 % FBS were seeded in the top chambers. Both top and bottom chambers contained the same concentrations of delivery systems. Cells were allowed to invade for 24 h. Non-invaded cells were scraped with cotton swab on the top surface of the membrane and invaded cells were fixed with methanol and stained with Griess solution. The membrane was left to dry in the air. Images were taken using an Olympus IX70 inverted microscope, the invaded cells were counted in five independent areas per membrane. The results were the means calculated from five replicates of each experiment. Three independent experiments were performed.

Animals

Male C57/BL/6 mice (6 weeks old) were purchased from Guangdong Medical Laboratory Animal Center (Guangzhou, China). The animals were kept in an environmentally controlled breeding room (temperature: 25 ± 1 ℃, relative humidity: 50 ± 5 %, 12 h dark/light cycle from 6:00 a.m. to 6:00 p.m.), with free access to sterilized tap water and commercial laboratory rodent chow. All animal experiment procedures were conducted in accordance with institutional and Chinese government guidelines for the care and use of experimental animals.

Matrigel plug assay

Matrigel (0.5 mL/plug) containing 300 ng VEGF and 150 units heparin with G2/PAH-Cit/SeNPs@siRNA (10 μg/mL) was injected (S.C.) into the ventral area of the 6 weeks old male C57/BL/6 mice (five mice per group). Matrigel mixed with medium alone was used as a negative control. After 14 days of implantation, the matrigel plugs were removed and the surrounding tissues were trimmed. The matrigel plugs were fixed and embedded with paraffin. Five-micron sections were stained by hematoxylin-eosin (H&E) stain. The number of erythrocyte-filled blood vessels in high power field (HPF; × 200.) was counted (plug number, 4-5). Three independent experiments were performed.

Aortic ring assay

96-well plates were covered with 50 μL Matrigel (supplemented with growth factor) at 4 ℃ and incubated at 37 ℃ for 30 min. Aortas isolated from mice were cleaned of periadventitial fat and connective tissues and cut into 1 to 1.5 mm long rings. After rinsing five times with medium, the aortas were placed on the Matrigel covered wells and covered with another 50 μL Matrigel. Aortic rings were cultured with different delivery systems. After 4 d of incubation, the microvessel growth was

quantified by taking photographs with an Olympus inverted microscope. After the images were acquired, the out-growth area was delineated and measured with Pro Plus soft-ware (Media Cybernetics).

In vivo and *Ex vivo* fluorescence imaging

All animal experiments (NO. SCXK2008-0002) were approved by the Institutional Animal Care and Use Committee of Jinan University. A549 cells (1×10^7) were injected subcutaneously into the right fore of the nude mice ages 5-6 weeks old. When the tumor volume reached 200-500 mm^3 (about 3 weeks after inoculation), 100 μg/kg of siRNA complexed to SeNPs or G2/PAH-Cit/SeNPs were intravenously injected into the mouse models with liver cancer via the tail vein. These mice were imaged at 0.5 h, 2 h, 4 h, 8 h, and 24 h post-injection by using IVIS Lumina imaging system (Xenogen (Caliper Life Sciences), Hopkinton, MA, USA). The fluorescence signals were acquired at a lateral position on the condition of 488-nm excitation filter and DsRed emission filter. Then, these mice were killed. The major organs, such as the liver, heart, lung, spleen, and kidney and the tumor, were collected to perform further fluorescence imaging observation.

Xenograft mouse model

The 5-week-old to 6-week-old severe combined immune deficiency (SCID) male mice (ordered from NIH) weighing ~20 g were divided into groups with five mice per group. A549 cells were s.c. injected (1×10^7 cells per mouse) into the mice. After the tumors had become established (~50 mm^3), the mice were s.c. injected with or without 100 μg/kg of siRNA complexed to SeNPs@siRNA or G2/PAH-Cit/SeNPs@siRNA everyday. The mice body weights and tumor sizes were recorded everyday, and the tumor sizes were determined by Vernier caliper measurements and calculated as length×width×height. After two weeks, mice with s.c. tumors not greater than 1.5 cm in diameter were sacrificed and Se concentrations were measured by ICP-AES.

Histopathology Evaluation

As described above, the spleen, liver, and kidney were dissected from the mice (21 days after treatment) for histopathological analysis. The paraffin-embedded tissues were cut at 5 μm thickness. The tissues were stained with hematoxylin and eosin (Sigma) to assess histological alterations by microscope. To evaluate the intratumoral microvessel density, the harvested tumors were fixed in 4% paraformaldehyde. Histological sections (8 mm thickness) were achieved using Freezing Microtome (Leica, Germany) and treated with paraformaldehyde for better fixation. After blocking with goat serum (10% in PBS), sections were further treated with CD31 (PECAM-1) antibody (Epitomics, America) followed by fluorescent secondary antibody and DAPI. We used a fluorescence microscope (Leica, Germany) through original magnification of 200-fold.

Results and discussion

Characterization of SeNPs and G2/PAH-Cit/SeNPs

G2/PAH-Cit/SeNPs were assembled layer-by-layer through electrostatic interactions.[32-34] SeNPs as cores for layer-by-layer assembly systems were prepared as previously described in the literature [29]，and PAH-Cit then was deposited onto the positively charged surface of SeNPs, obtained PAH-Cit/SeNPs with negatively charged, deposition of G2 PAMAM on the PAH-Cit/SeNPs was

done in the last step. siRNA should present on the surface of the delivery vector through electrostatic interactions. The two sequential reversals of zeta-potential indicated successful deposition of G2 and PAH-Cit onto the surface of the SeNPs (Fig.S2). The characteristics of the delivery systems were determined by TEM (Fig.1A). These data showed that all of the nanoparticles were well dispersed and the average particle size of the SeNPs was 74.5 nm with the particle size of G2/PAH-Cit/SeNPs increasing to 102.8 nm. The SeNPs@siRNA and G2/PAH-Cit/SeNPs@siRNA delivery systems had an increase in average particle size to 87.4 nm and 111.5 nm, respectively (Table S1). An elemental composition analysis employing EDX of SeNPs and G2/PAH-Cit/SeNPs showed the presence of a strong signal from the Se atoms (48.02 % and 22.98 % respectively) (Fig.S2).

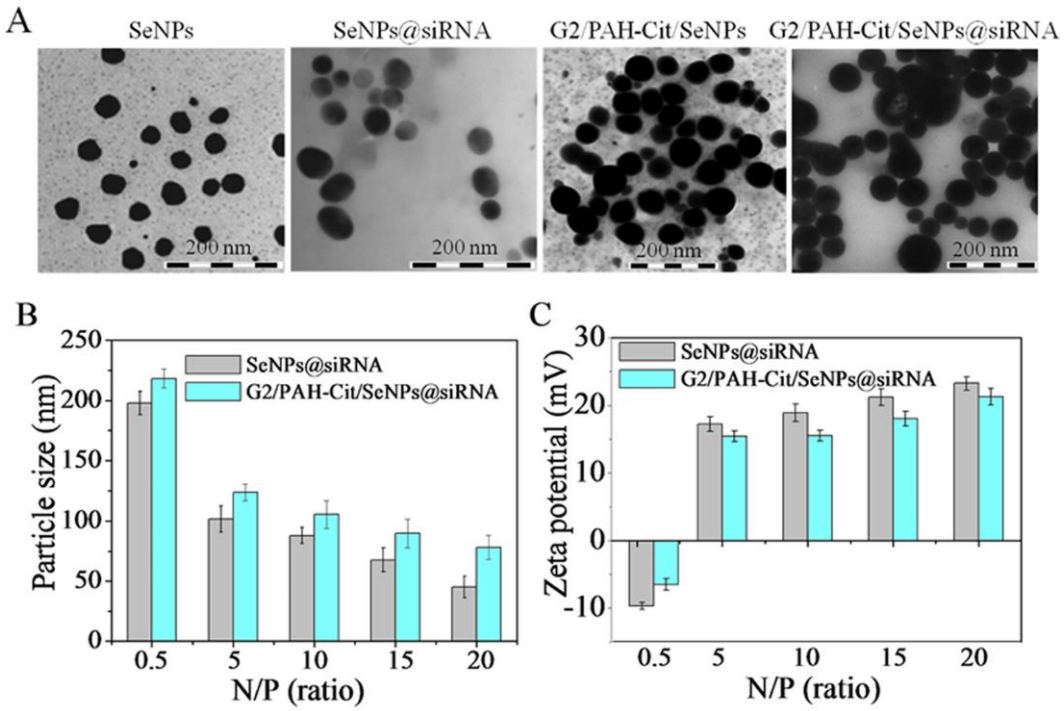

Fig.1. Structural characterization of SeNPs delivery systems. (A) TEM micrograph of SeNPs. (B) Hydrodynamic diameter distribution and (C) zeta potential of SeNPs@siRNA and G2/PAH-Cit/SeNP@siRNA of various N/P ratios at 37℃. Data are shown as mean ± S.D. (n = 3).

We measured the particle sizes and zeta potentials of SeNPs@siRNA and G2/PAH-Cit/SeNPs@siRNA delivery systems at N/P ratios ranging from 0.5 : 1 to 20 : 1. As shown in Fig.1B, the particle size of G2/PAH-Cit/SeNPs@siRNA showed a significant decline when the N/P ratio was raised from 0.5 : 1 to 5.0 : 1, but this rapid decline gave way to a more gradual decrease as the ratio was changed from 5.0 : 1 to 20 : 1. Within this latter range, all particle sizes remained around 100 nm. Inversely, we saw an increase in zeta potentials as the N/P ratio increased, indicated by the potential reading of -10.6 mV seen at an N/P ratio of 0.5 : 1 versus 15.4 mV seen at

an N/P ratio of 5.0 : 1, while a lesser degree with increasing N/P ratios of G2/PAH-Cit/SeNPs@siRNA (Fig.1C). In other words, the zeta potential change of SeNPs@siRNA was similar to the G2/PAH-Cit/SeNPs@siRNA delivery system. These data indicate that strong electrostatic binding occurred between G2/PAH-Cit/SeNPs and siRNA and that stable nanoparticles were formed at G2/PAH-Cit/SeNPs@siRNA N/P ratios of 5.0 : 1 and above.

siRNA binding affinities and stability of the delivery systems

Cationic poly(amidoamine) (PAMAM) dendrimers were widely used as nonviral gene carriers, but with high cost and serious cytotoxicity.[35] Here, we developed G2/PAH-Cit/SeNPs delivery system, which combined the loading capacity of G2 PAMAM with large specific surface and good biocompatibility of SeNPs. We sought to find the potential of G2/PAH-Cit/SeNPs in loading and delivery capacity of genes. We selected plasmid DNA (pDNA) as a model gene, as this has been one of the most fascinating genetic molecules.[36,37] We performed agarose gel electrophoresis with vector to pDNA N/P ratios ranging from 0.5 : 1 to 8.0 : 1. As shown in Fig.2A, G2/PAH-Cit/SeNPs possessed a better DNA binding ability, resulting in a completely condensed plasmid at an N/P ratio of 2.0 : 1. However, the migration of pDNA was completely prevented when complexes were formed at an N/P ratio of 4.0 : 1 and 8.0 : 1 for G5 and G2 and SeNPs, respectively. The results have been proved that G2/PAH-Cit/SeNPs had haigher loading capacity than G2 and G5, SeNPs also had certain ability to load pDNA, but obviously weaker than G2/PAH-Cit/SeNPs.

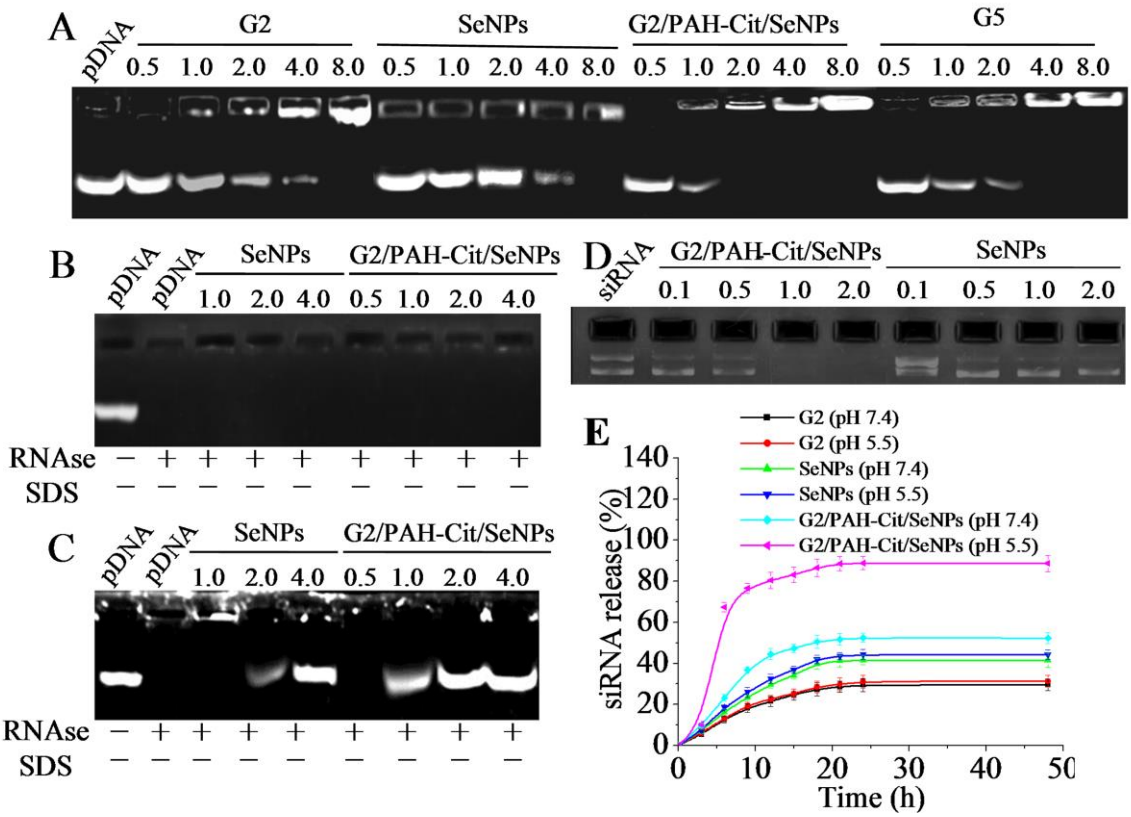

Fig.2. (A) Agarose gel electrophoresis of materials of naked pDNA and nanoparticles@pDNA at various N/P ratios

(0.5:1, 1.0:1, 2.0:1, 4.0:1, and 8.0:1). (B) Agarose gel electrophoresis of nanoparticles at 56 V for 1 h after incubation with RNase A. (C) Agarose gel electrophoresis of nanoparticles at 56 V for 1 h after treatment with RNase A and SDS. (D) Agarose gel electrophoresis of materials of naked siRNA and nanoparticles@siRNA at various N/P ratios (0.1:1, 0.5:1, 1.0:1, and 2.0:1). (E) Release profiles of FITC-siRNA from materials prepared at vector/siRNA mass ratios of 5:1 in pH 7.4 and pH 5.5, 0.2 M PBS at 37℃.

The stabilities of G2/PAH-Cit/SeNPs@pDNA delivery system were then examined by RNase digestion, thereby mimicking physiological conditions. When the sample was further treated with RNase A, uncomplexed pDNA (Fig.2B, lane 1) was detected through ethidium bromide staining. Once the pDNA was either degraded by RNase (Fig.2B, lane 2) or completely bound to the gene delivery systems (Fig.2B, lanes 3-9), no band appeared. These results indicate that both SeNPs and G2/PAH-Cit/SeNPs can protect the pDNA from RNase degradation. To further support these data, Fig.2C shows the release of pDNA through the action of SDS on the pDNA bound to either gene delivery system after an initial RNase digestion. Furthermore, the fluorescence intensity gradually increased linearly with the N/P ratio from 1.0 : 1 to 4.0 : 1, further suggesting that released pDNA was protected by the nanoparticles of the G2/PAH-Cit/SeNPs system. These results show that the conjugation of gene to G2/PAH-Cit/SeNPs can effectively protect gene from enzymatic degradation.The different ability to condense DNA and siRNA was related to different molecular weight of nucleic acid. However, G2/PAH-Cit/SeNPs complete retardation of siRNA was achieved above the w/w ratios of above the N/P ratios of 1.0 : 1, and the migration of siRNA was not completely prevented when SeNPs with siRNA were formed at an N/P ratio of 2.0 : 1. Therefore, the condition for layer deposition is carefully established to enableG2/PAH-Cit/SeNPs with high ability to bind nucleic acid.

siRNA loading and release from the delivery systems *in vitro*

We observed that the maximum loading capacity of siRNA onto the nanoparticles and the proper loading time. For all the samples, the quantity of siRNA was 10μg, the N/P ratios of SeNPs or G2/PAH-Cit/SeNPs to siRNA were 1.0 : 1, 5.0 : 1, 10.0 : 1, respectively. As shown in Fig.S3, both SeNPs and G2/PAH-Cit/SeNPs had loading capacity to siRNA at different N/P ratios, the loading quantity of siRNA increased sharply within the first 15 min and changed slightly in the following 15 min, and the N/P ratio of vector : gene affected the loading quantity of siRNA, and the optimal loading was determined at the N/P ratio of 5.0 : 1. When the N/P ratio at 5.0 : 1, the maximal siRNA loading quantity of G2/PAH-Cit/SeNPs and SeNPs reached to 7.41 μg and 3.78 μg, respectively, at approximately 30 min, indicating that G2/PAH-Cit/SeNPs and SeNPs had a loading capacity of siRNA of approximately 74.1 % and 37.8 %, respectively (～1.96 times higher in G2/PAH-Cit/SeNPs). The loading conditions were thus determined at N/P ratio of delivery system : siRNA 5.0 : 1 and a loading time 30 min for further gene delivery and cell studies.

To validate the functionality of charge-reversal of PAH-Cit, the G2/PAH-Cit/SeNP@siRNA delivery system was incubated at a range of pH values from 5.5 and 7.4. The amount of siRNA (fluorescein isothiocyanate (FITC)-labeled) released into the supernatant was then determined by measuring the fluorescence excitation at

488 nm at different time points. After 9 h of incubation, the cumulative siRNA released from G2/PAH-Cit/SeNPs reached 77.4 % at pH 5.5 but only 23.2 % at pH 7.4 (Fig.2E). The siRNA maximum release efficiencies of G2/PAH-Cit/SeNPs@siRNA nearly reached 88% after 18 h of incubation. SeNPs that are not charge-reversible showed a similar release curve at both pH 7.4 and pH 5.5, with only 43 % siRNA released after 24 h. The results showed that G2/PAH-Cit/SeNPs had not only high loading capacity but also excellent release efficiency. These results attributed the release of siRNA to facilitate by the charge-shifting character of PAH-Cit, which conversion from an anionic to a cationic character in an acidic environment disrupted the layer-by-layer structure of the complex, thus facilitating release.

Cell viability assay

The cytotoxicity of these delivery systems was screened against series types cells: HeLa, A549, and HepG2, HUVEC and NIH/3T3 by an MTT assay. There was no apparent toxicity observed for siRNA, SeNPs and G2/PAH-Cit/SeNPs within all cell lines (Table 1). However, HUVEC and A549 cells both exhibited higher toxicity when treated with SeNPs@siRNA and G2/PAH-Cit/SeNPs@siRNA, with IC_{50} values in A549 cells being 21.45 and 8.74, respectively. These results verify that the decreased cell viability was caused by VEGF-specific gene knockdown and not by delivery system- induced cytotoxicity. Moreover, layer-by-layer assembly of G2/PAH-Cit/SeNPs reduced the toxicity of G2 PAMAM dendrimers and increased the efficiency of VEGF-gene silencing.

Table 1. Cytotoxic effects of delivery systems on cells.

	IC_{50} [μg/mL]				
Delivery systems	HeLa	HUVEC	HepG2	A549	NIH/3T3
siRNA	>200	>200	>200	>200	>200
SeNPs	91.45 ±1.03	83.25 ± 0.41	93.85 ± 1.22	92.21 ± 2.66	>200
G2/PAH-Cit/SeNPs	97.54 ±1.61	78.75 ±0.55	100 ± 3.82	65.43 ± 3.52	184.36 ±4.96
SeNPs@siRNA	68.16 ±0.86	25.62 ±0.68	75.25 ± 2.63	21.45 ±1.58	142.43 ±3.74
G2/PAHCit/SeNPs@siRNA	72.02 ±1.57	6.52 ± 0.23	59.87 ± 0.88	8.74 ±0.39	135.38 ±2.79

***In vitro* transfection efficacy of delivery systems**

Gene transfection efficacy of G2/PAH-Cit/SeNPs was measured with enhanced green fluorescent protein (EGFP) gene in both A549 and HUVEC cells. Among the tested delivery systems, exogenous EGFP transfection with G2/PAH-Cit/SeNPs showed much higher gene transfection efficacy than G2, SeNPs, or dendrimer generation 5 (G5) at different N/P ratios in A549 cells (Fig.3A), cells incubated with G5@EGFP polyplex showed highest transfection efficacy at an N/P ratio of 10:1 due to the cytotoxicity of G5 at high concentrations. In addition, G2/PAH-Cit/SeNPs at an N/P ratio of 10:1 exhibited higher EGFP transfection efficacies than SeNPs, even at an N/P ratio of 20:1. Similar results we observed in Fig.3C for HUVEC cells. These results indicate that

G2/PAH-Cit/SeNPs significantly improved the efficiency of gene transfection compared to SeNPs at an N/P ratio of 10 : 1, we use the ratio in the next cell experiments.

To specifically determine the EGFP transfection level in cells, the average fluorescence intensity of each sample was measured by flow cytometry, and the relative quantitative assay was shown in Fig. 3B and Fig.3D. The greatest EGFP expression level in A549 cells treated with SeNPs@siRNA was 19.5 % at N/P ratio of 20 : 1 comparable to G5 PAMAM (12.8 % at N/P ratio of 10 : 1). EGFP expression level in A549 cells treated with G2/PAH-Cit/SeNPs@siRNA was nearly 58.5 % at N/P ratio of 10 : 1, indicating a remarkably high transfection efficiency. The EGFP expression level in HUVEC cells treated with delivery systems had similar results to expression level in A549 cells.

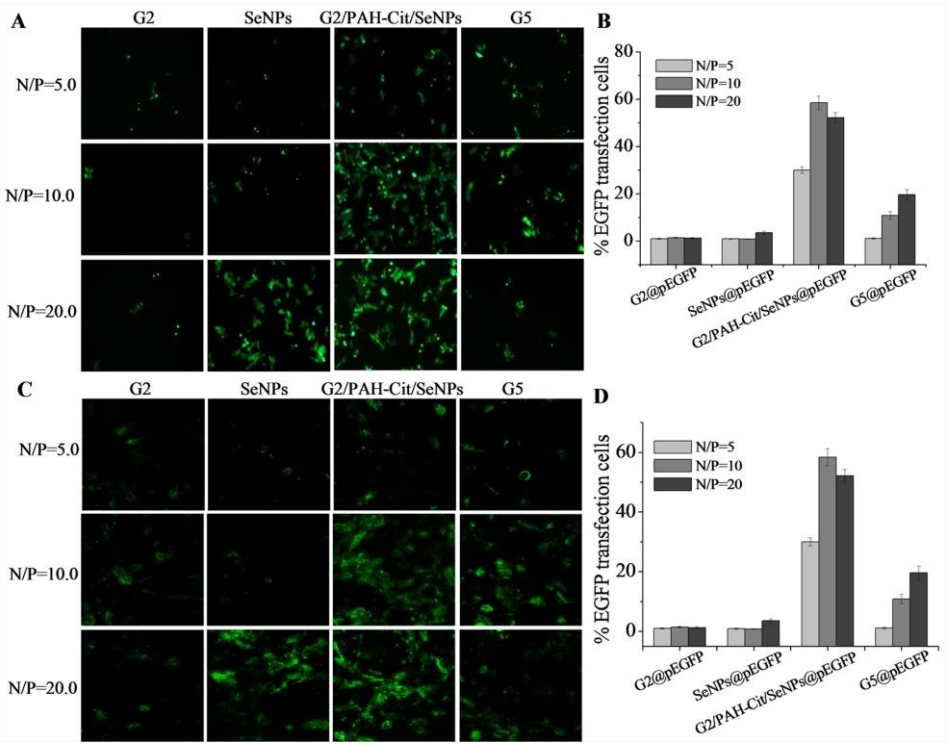

Fig.3. Fluorescent microscopy images of A549 cells (A) and HUVEC cells (C) transfected by G2, SeNPs, G2/PAH-Cit/SeNPs and G5 for 24 h. EGFP plasmid expressions were observed in green fluorescence. The N/P ratios of the polyplexes were 5:1, 10:1, and 20:1, respectively. The EGFP gene transfection efficacy (%) A549 cells (B) and HUVEC cells (D) was determined from flow cytometry.

Intracellular localization of G2/PAH-Cit/SeNPs and release of siRNA in cytoplasm

The cellular uptake and intracellular localization of a gene carrier play important roles in successful gene transfection. To assess the cellular uptake of SeNPs@siRNA and G2/PAH-Cit/SeNPs@siRNA, FITC-labeled siRNA molecules were utilized to prepare G2/PAH-Cit/SeNPs@siRNA. Flow cytometric analysis revealed that the fluorescent intensity of A549 cells

incubated with naked siRNA only weakly increased (Fig.4A). Comparatively the fluorescent intensities of FITC-siRNA delivered by G2/PAH-Cit/SeNPs were significantly higher than SeNPs, with mean intensities of 1135±32.4 and 1860±46.3, respectively. We also examined the cellular uptake of SeNPs@siRNA and G2/PAH-Cit/SeNPs@siRNA delivery systems in HUVEC cells by using ICP-AES analysis. As shown in Fig.4B, HUVEC cells treated with 5 μg/mL G2/PAH-Cit/SeNPs had significantly increased Se concentrations, from 0.0043 in control conditions to 3.0 μg/10^7 cells. This result was significantly higher than that of SeNPs (1.4 μg/10^7 cells), indicating that G2/PAH-Cit/SeNPs could effectively increase cellular uptake and agreeing with our prior results from our flow cytometric analysis. Taken together, our results suggest that the assembly of G2/PAH-Cit/SeNPs promotes the celluar uptake of siRNA with reduced cytotoxicity.

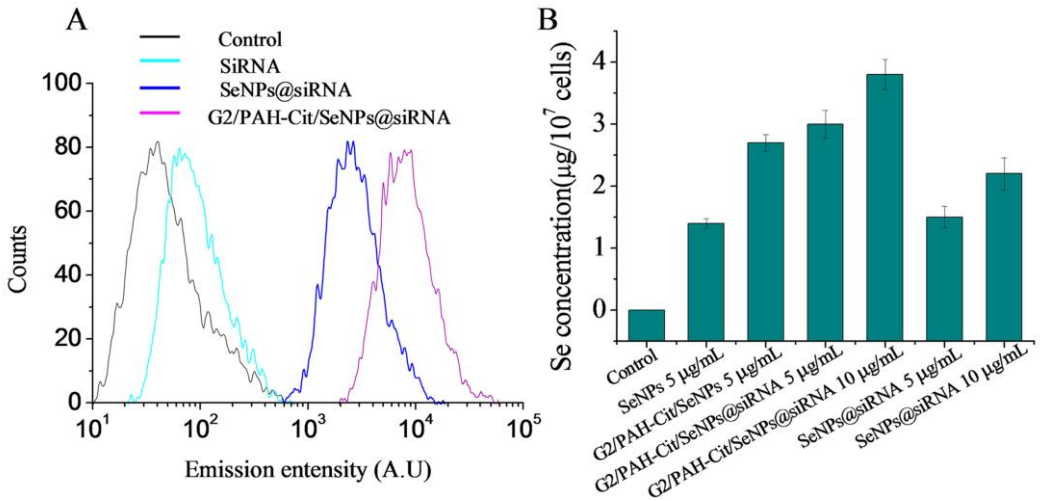

Fig.4. (A) Cellular uptake of different amounts of FITC-siRNA with different delivery systems was analyzed 6 h post-transfection by flow cytometry. (B) Quantitative analysis of Se concentrations in HUVEC cells exposed to delivery systems for 6 h by ICP-AES method.

To track the distribution of gene delivery systems following cellular uptake, A549 cells were treated with different delivery systems 6 h and individually stained with Lysotracker Red (red fluorescence). As shown in Fig.5A, there was limited green fluorescence inside cells treated with FITC-siRNA only, demonstrating that FITC-siRNA alone is difficult to enter and accumulate in cells. The G2@siRNA and G5@siRNA complexes were then attached to the cell membrane and were observed as a bright, green fluorescent ring around the cells. We also observed colocalization (indicated by yellow color) of the red and green fluorescence signals in cells treated with SeNPs@siRNA. It is worth noting that after G2/PAH-Cit/SeNPs@siRNA incubation, the diffuse red fluorescence not only had extensive colocalization with the LysoTracker Red probe, but also exhibited a diffuse pattern of localization within the cytoplasm. We hypothesized that the G2/PAH-Cit/SeNPs@siRNA would first accumulate in the lysosomes, and, as time elapsed,

G2/PAH-Cit/SeNPs@siRNA would be released into the cytoplasm.

To confirm whether siRNA could be released from lysosomes, we further observed the intracellular locations of siRNA at different time points. As shown in Fig.5B, as incubation time increased, G2/PAH-Cit/SeNPs@siRNA was gradually transported into cells and its location within lysosomes increased in a time-dependent manner. To this end, limited colocalization signals appeared in the merged image after 8 h of incubation, indicating that most of the siRNA molecules were released from the lysosomes. This result can be attributed to the increased ability of the G2/PAH-Cit/SeNPs@siRNA delivery system to escape from the lysosomes.

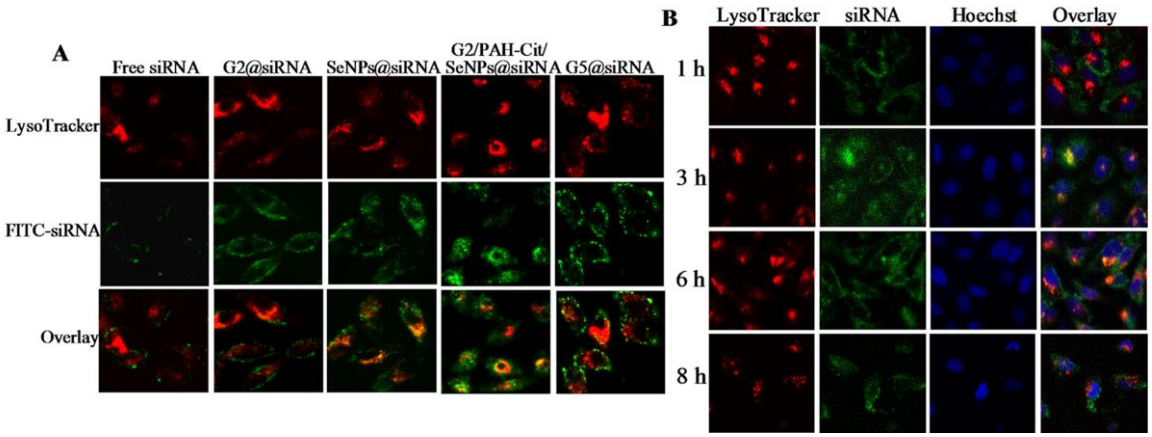

Fig.5. Colocalization of delivery systems (green fluorescence) and lysosomes (red fluorescence) in A549 cells. (A) The A549 cells were treated with naked siRNA, G2@siRNA, SeNPs@siRNA, G2/PAH-Cit/SeNPs@siRNA and G5@siRNA for 6 h. (B) The A549 cells were treated with G2/PAH-Cit/SeNPs@siRNA for different periods of time and visualized under a laser confocal microscopy.

We were also able to show the cellular localization at different time points post-incubation of G2/PAH-Cit/SeNPs@siRNA in live cells using transition electron microscopy (TEM). Fig.6A and Fig.6B not only show the attachment of aggregated G2/PAH-Cit/SeNPs@siRNA to the membrane of A549 cells, but also the presence of G2/PAH-Cit/SeNPs@siRNA in endosomal and lysosomal compartments after 1h of incubation. These data confirm that the G2/PAH-Cit/SeNPs@siRNA was transported into cells via an endocytotic pathway. As incubation time increased, G2/PAH-Cit/SeNPs@siRNA was taken up by A549 cells and was well-distributed within the cytosol at 6 h, without the formation of large aggregates. Interestingly, after 24 h of incubation in A549 cells, nanoparticles were found clustered in cellular compartments that appeared to be within the nucleus. Based on the previously described anti-cancer activities and low toxicity of SeNPs,[26] we hypothesized that SeNPs localized within the nucleus induced cell apoptosis after G2/PAH-Cit/SeNPs@siRNA released its siRNA cargo into the cytosol. To sum up, G2/PAH-Cit/SeNPs@siRNA has been higher cellular uptake efficiency, the charge reversion of PAH-Cit under acidic environment facilitates of delivery system, thereby

facilitating escape from the endolysosomes and release the loaded siRNA molecules into cytoplasm, thereby mediating remarkable interference effect on target gene in tumor cell.

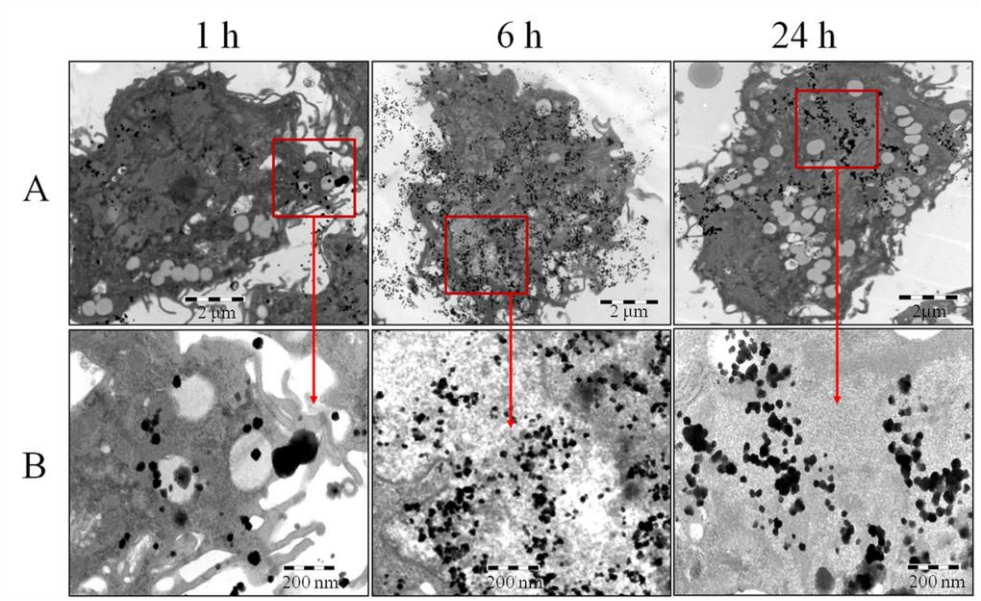

Fig.6. (A) TEM images of A549 cells treated with 10 μg/mL G2/PAH-Cit/SeNPs for 1 h, 6 h and 12 h respectively. (B) Representative high magnification TEM micrographs of a part of A549 cells for 1 h, 6 h and 12 h, respectively.

***In vitro* effects of knockdown of cancer-related gene products**

It is well known that the vascular endothelial growth factor (VEGF) is a key regulator of physiologic angiogenesis and plays a major role in the pathobiology of cancer.[38] Based on selenium nanoparticles having both a greater tumor-targeting efficacy and inhibition of tumor growth and angiogenesis, we tried to use G2/PAH-Cit/SeNPs@siRNA to suppress the VEGF gene expression for inhibition of tumor growth and metastasis in cancer treatments.

To evaluate the power of targeted gene silencing of the G2/PAH-Cit/SeNPs@siRNA delivery system, we examined its inhibitory activity of VEGF expression in HUVEC cells through Western Blot and chosen suramin as a positive control.[39,40] As shown in Fig.7A, cells treated with G2@siRNA, G2/PAH-Cit/SeNPs@siRNA, SeNPs@siRNA, G5@siRNA induced significative degrees decreases in VEGF protein levels when compared to cells treated with either control or naked siRNA. Importantly, the protein levels of cells treated with G2/PAH-Cit/SeNPs@siRNA had a larger decrease (81.3 %) than those treated with suramin (68.4 %) indicating that G2/PAH-Cit/SeNPs could load siRNA very effectively (Fig.7C).

The VEGFRs are structurally related members of the RTK family that mediate critical signaling pathways in endothelial cells. For pVEGFR-2, protein expression of pVEGFR2 was significantly suppressed after treatment with G2/PAH-Cit/SeNPs@siRNA (Fig.7D). Although gene expression after treatment with SeNPs and G2/PAH-Cit/SeNPs carrying XsiRNA which is scrambled control had weak knockdown, this result is likely not due

to XsiRNA gene expression, but rather SeNPs anti-tumor activity. The above results demonstrate the specificity of siRNA-mediated silencing through G2/PAH-Cit/SeNPs@siRNA and its ability to inhibit angiogenesis through a down-regulation of VEGF and pVEGFR-2 expression.

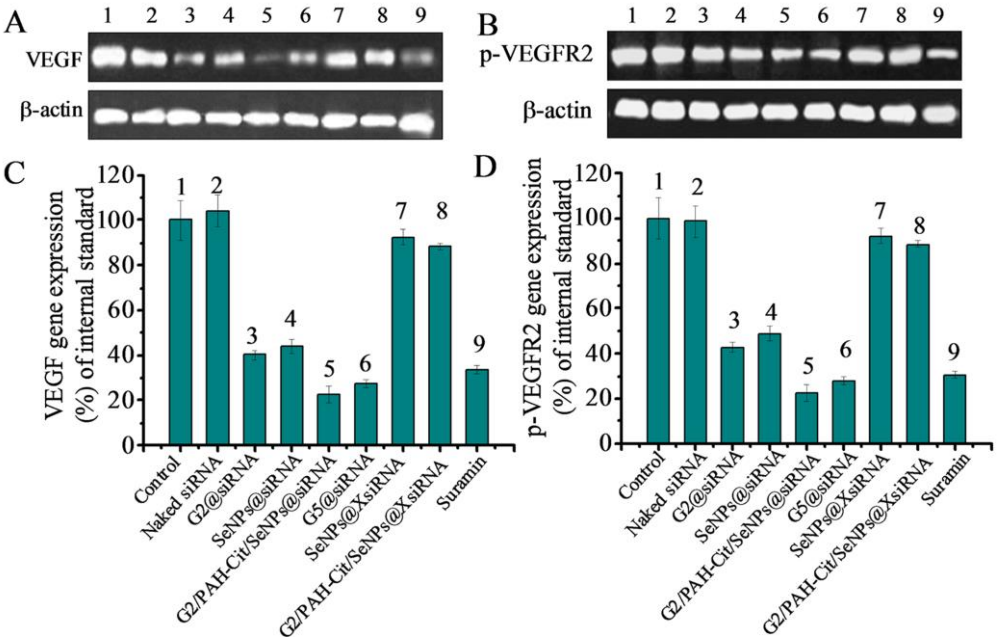

Fig.7. (A and C) Level of VEGF expression for HUVEC cells after treatment with different delivery systems 10 μg/mL for 48 h. β-action was used as internal reference. (B and D) Protein level of p-VEGFR2 and β-action in A549 tumor cells.

Delivery systerms inhibit VEGF-induced invasion and tube formation of endothelial cells

The ability of a tumor to metastFasize is related to the degree of angiogenesis it induces.[41] To investigate the effect of delivery systems on endothelial cell tube formation, we did both a Matrigel and Transwell assay. As shown in Fig.S4A, G2/PAH-Cit/SeNPs@siRNA showed a robust inhibitory effect on tube formation (Fig.S4C), inhibiting 46.2 % of tube formation in siRNA-treated HUVEC cells. Furthermore, G2/PAH-Cit/SeNPs@siRNA significantly inhibited VEGF-induced HUVECs invasion, reaching 81% at a concentration of 20 μg/mL (Fig.S4B and Fig.S4D). However, naked siRNA exhibited almost no inhibitory effects in the Transwell assays. Although tube formation after treatment with G2/PAH-Cit/SeNPs@XsiRNA had a weak inhibitory effect, this result was not due to XsiRNA gene expression, but rather the inhibition of angiogenic ability of SeNPs.

G2/PAH-Cit/SeNPs@siRNA inhibits angiogenesis *in vitro* and *in vivo*

To further investigate the anti-angiogenesis effect of G2/PAH-Cit/SeNPs@siRNA, we performed aortic ring

assays using isolated aortas from mice. From the MTT assay, there was no apparent toxicity observed for SeNPs within all cell lines, HeLa, A549, and HepG2, HUVEC and NIH/3T3 and ICP-AES analysis revealed that cellular uptake of SeNPs in cells was also limited. SeNPs inhibits angiogenesis *in vitro* and *in vivo* was not shown here. As shown in Fig.8A, VEGF in Matrigel can dramatically induce microvessel sprouting, whereas addition of 10 μg/mL G2/PAH-Cit/SeNPs@siRNA significantly blocked VEGF-induced microvessel sprouting. This effect was approximately 80%-a larger blockage than aortas treated with suramin (Fig.8B), naked siRNA and G2/PAH-Cit/SeNPs@XsiRNA treated group also weakly blocked VEGF-induced microvessel sprouting compared to control. We investigated whether the anti-angiogenesis actions of G2/PAH-Cit/SeNPs@siRNA would also be expressed *in vivo* using a Matrigel plug assay. Matrigel plugs containing VEGF were excised from mice. They were dark red and filled with blood vessels, indicating that functional vasculatures had formed (Fig.8C). Matrigel plugs from mice treated daily with VEGF plus G2/PAH-Cit/SeNPs@siRNA had a significantly paler appearance, indicating less blood vessel formation. Histological analysis using hematoxylin and eosin (H&E) staining showed that G2/PAH-Cit/SeNPs@siRNA strongly inhibited the number of vessels and the formation of microvessels when compared to those treated with only VEGF (Fig.8D). Together, these results indicated that G2/PAH-Cit/SeNPs@siRNA is capable of inhibiting VEGF-induced neo-vessel formation both *in vitro* and *in vivo*.

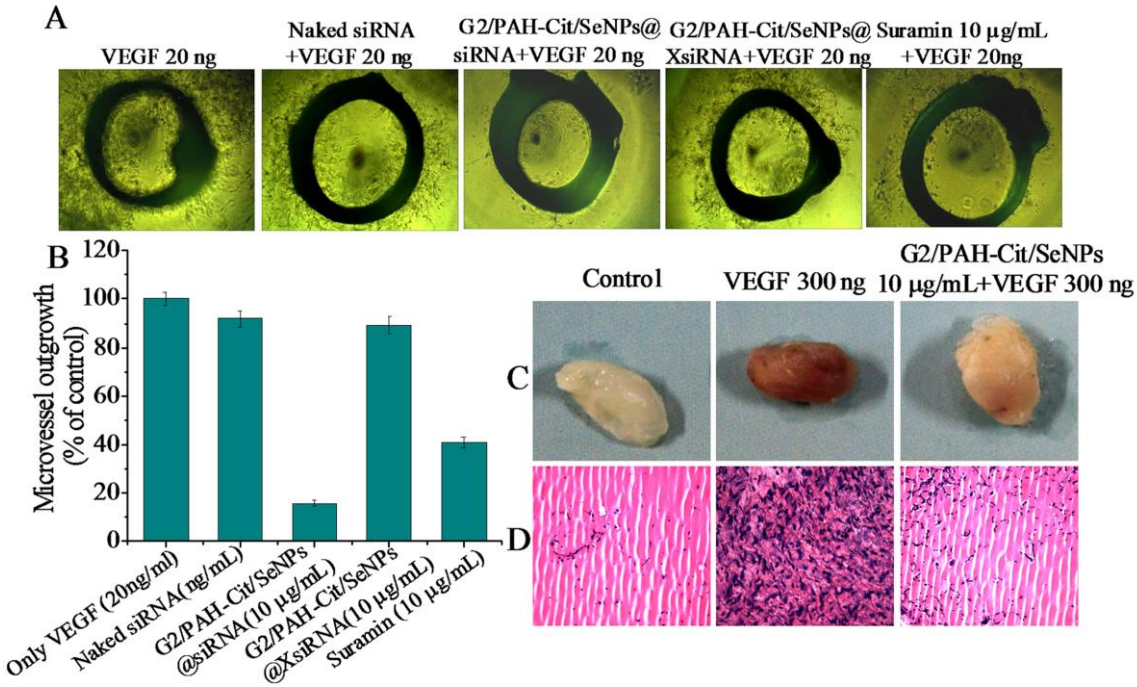

Fig.8. G2/PAH-Cit/SeNPs@siRNA inhibits microvessel sprouting ex vivo and angiogenesis *in vivo*. (A and B) Morelloflavone inhibits microvessel sprouting in mouse aortic ring assay. Aortic segments isolated from Spraguee-Dawley rats were placed in the Matrigel-covered wells and treated with 300 ng VEGF in different 10 μg/mL delivery systems. (C) G2/PAH-Cit/SeNPs@siRNA inhibits angiogenesis in Matrigel plug assay. Six-week-old C57/BL/6 mice were injected with 0.5 μL of Matrigel containing 10 μg/mL G2/PAH-Cit/SeNPs@siRNA, 300 ng of VEGF, and 20 units of heparin into the ventral area (n=5 per group). After 6 d, representative Matrigel plugs were removed and

photographed. (D) The Matrigel plugs were fixed with formalin and 5-μm sections were stained with H&E (magnification, ×200) staining in C.

In vivo fluorescent imaging and biodistribution

As an effective delivery system for anti-cancer agents, a potential carrier should be able to deliver the drugs directly into tumor tissues to achieve the tumor-targeted therapy.[15,42,43] To evaluate whether G2/PAH-Cit/SeNPs@siRNA nanoparticles could efficiently assist in siRNA accumulation in tumors, we evaluated the time-dependent bio-distribution of different siRNA formulations in a xenograft mouse model by fluorescent imaging.

IVIS Lumina imaging system which we used for *in vivo* imaging could remove the tissue autofluorescence and subtract the background at a certain degree. Through the system modulated, there were no signals in the tumor tissues in the blank group (not injected G2/PAH-Cit/SeNPs@siRNA), suggesting no auto fluorescence interfere *in vivo* images and the fluorescence signal intensity of *in vivo* imaging is close to a true reflection of the G2/PAH-Cit/SeNPs@siRNA retained inside the organs. As presented in Fig.9A, the real-time images of G2/PAH-Cit/SeNPs@siRNA in the tumor-bearing control mice show the whole bodies of the control mice group, monitored at 0.5 h, 2 h, 4 h, 8 h and 24 h after intravenous injection. During this live imaging test, there was obvious tumor tissue in the mice armpit.

Fluorescent signals in the liver and kidney originating from FITC-siRNA were observed 0.5 h after G2/PAH-Cit/SeNPs@siRNA was administered to the mice. The fluorescence signals clearly accumulated in both the liver and kidney, but weak to non-existent fluorescent signals were detected in the tumor tissue itself. After two hours, the fluorescence signal became visible and gradually increased within the tumor tissue. The signal attained maximum intensity after 4 h, but the tumor fluorescent intensity dramatically decreased after 24 h had elapsed. Meanwhile, we observed that the fluorescence intensity of G2/PAH-Cit/SeNPs@siRNA treat mice at 4 h after the last injection. Although the tumor tissue itself was small, accumulation of fluorescence was also observed in the tumor site besides the liver or other normal tissues.

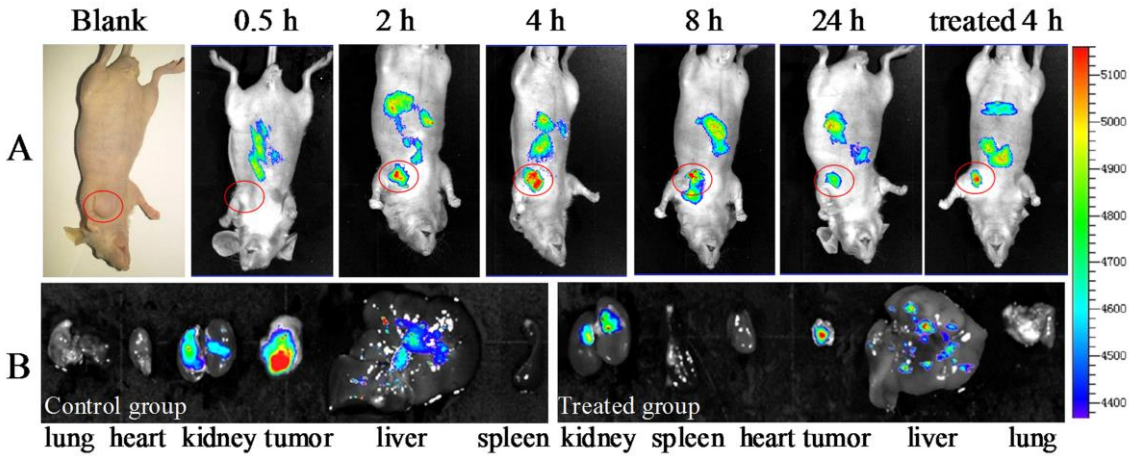

Fig.9. (A) *In vivo* imaging of tumor-bearing mice after administration of G2/PAH-Cit/SeNPs@siRNA at 0.5 h, 2 h, 4 h, 8

h and 24 h. (B) Ex vivo fluorescence images of tissues including heart, liver, spleen, lung, kidney and tumor collected at 4 h post-injection of G2/PAH-Cit/SeNPs@siRNA (left as control and right as G2/PAH-Cit/SeNPs@siRNA treated).

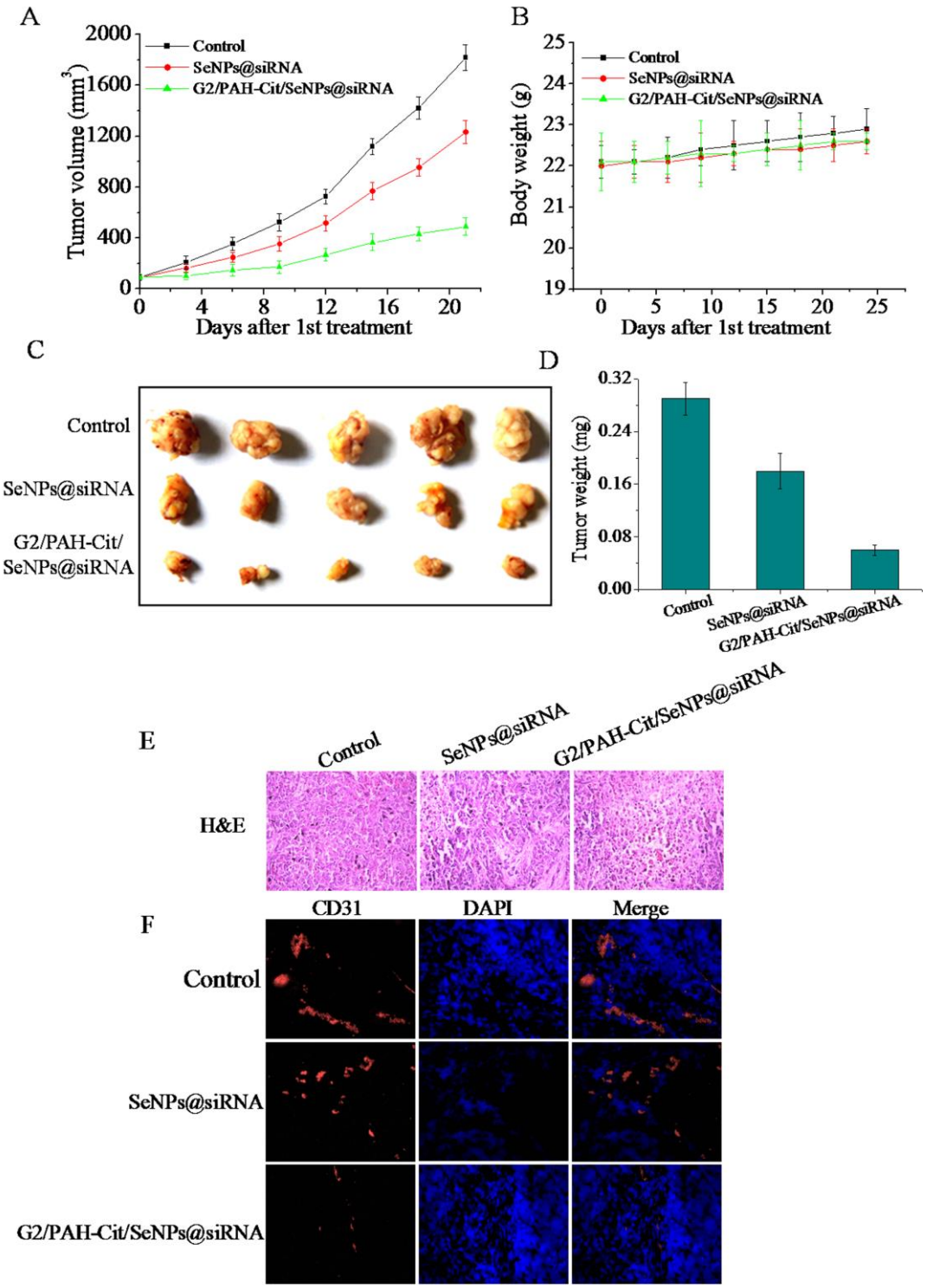

Fig.10. (A) Tumor volumes at different times after tumor inoculation. The tumor volumes were calculated by $V=lw^2/2$ (mean±SD, n = 5 animals per group). (B) The average mouse body weight was monitored with electronic balance every

3 days. (C) The images of dislodged tumors from the mice of five groups after last injection. (D) The weight of dislodged tumors from the mice of five groups. (E) H&E stained images of tumor with collected from SeNPs@siRNA or G2/PAH-Cit/SeNPs@siRNA injected mice and control treated mice with PBS. Scale bar = 50 μm. (F) Representative photographs of immunofluorescent staining of vascular endothelial cells with the CD31 antibody. The red and blue fluorescence represented the CD31-positive vessel and the nuclei of cells, respectively. Photographs were taken at original magnification of ×200.

To provide more direct evidence, mice were sacrificed and major organs (e.g. heart, liver, spleen, lung, kidney and tumor) were excised and fluorescence images were taken with an *in vivo* imaging system (Fig.9B). Whether the control or delivery systems treated groups, fluorescent signals were strongly associated with the tumor tissue, thus further confirming the previously observed fluorescence signals in living mice. Except for the liver and kidney, which showed weak accumulation, uptake into other tissues such as the lung and spleen was minimal. This increase in tumor-targeting efficiency provided by nanoparticle delivery might be due to an enhanced permeability and retention (EPR) effect. Our results indicate that G2/PAH-Cit/SeNPs@siRNA has enhanced tumor-targeted delivery and quicker uptake into tumor cells providing for more efficient gene silencing.

In vivo anti-tumor effect

The *in vivo* gene silencing efficacy of G2/PAH-Cit/SeNPs@siRNA was further evaluated by monitoring tumor growth in an animal xenograft model. We predicted that our delivery system would be able to suppress tumor growth and angiogenesis in this model. Due to a weak anti-cancer effect of SeNPs, We no longer researched the anti-tumor effect *in vivo*. The mice were then intravenously injected with 100 μg/kg of siRNA complexed to SeNPs and G2/PAH-Cit/SeNPs. Injections occurred for a total of seven times on alternate days and both mouse body weights and tumor size were recorded simultaneously. The non-treatment control group was injected with 100 μL of PBS in the same manner. After 24 days, mice were sacrificed, the tumor weights were calculated, and sections of various organs (e.g. heart, lung, liver, spleen and kidney) were subjected to physiological analysis.

The average volume of tumor was monitored every three days, as shown in Fig.10A, with the increase of treat time with SeNPs@siRNA or G2/PAH-Cit/SeNPs@siRNA, the volume of tumor groups were obviously reduced. The average volume of the tumors treated with SeNPs@siRNA and G2/PAH-Cit/SeNPs@siRNA reached 1192±96.2 mm^3 and 490±89.4 mm^3 at Day 21, respectively. Now, tumor growth inhibition reached 34.2 % and 79.4 % respectively, as compared to tumors from the control group, which had a mean volume of 1816±102.5 mm^3. It can be seen that G2/PAH-Cit/SeNPs@siRNA has very good effect on inhibiting tumor growth. Furthermore, we also monitored the weight of mice at every three days, no significant body weight loss was observed after the administration of either SeNPs@siRNA or G2/PAH-Cit/SeNPs@siRNA (Fig.10B), showing that both delivery systems were well-tolerated at the tested dose.

Fig.10C showed the solid tumors stripped out the mice. Intuitively, treatment with SeNPs@siRNA resulted in a modest, albeit significant reduction, of tumor size, compared with the control group, and treatment with G2/PAH-Cit/SeNPs@siRNA significantly inhibits tumor growth. From the weight of these tumors at Day 21, the

mean weight of SeNPs@siRNA and G2/PAH-Cit/SeNPs@siRNA treated groups only reached 0.18 mg and 0.05 mg respectively, as compared to tumors from the control group reached 0.29 mg (Fig.10D). The results could further proved that G2/PAH-Cit/SeNPs@siRNA had significantly inhibited the growth of the tumor. These results demonstrate that the G2/PAH-Cit/SeNPs@siRNA delivery system has a greater ability for efficient siRNA release when compared to SeNPs@siRNA, thereby giving it a greater capacity for gene silencing. The charge reversion delivery system G2/PAH-Cit/SeNPs had stronger binding affinities with siRNA and release efficiency than SeNPs, This result could be attributabled to high loading efficiency of G2 dendrimers and charge reversion at acidic environments of PAH-Cit.

The histological changes of tumor tissue that resulted from the different delivery systems were compared using the ex vivo H&E staining assay. Control tissue appeared to be predominantly hypercellular and showed obvious nuclear polymorphisms and foci of hemorrhage. Tumor tissues from the animals treated with G2/PAH-Cit/SeNPs@siRNA showed fewer tumor cells and had higher levels of apoptosis in conjunction with chromatin condensation or nuclei fragmentation when compared to those treated with SeNPs@siRNA. Again, these results indicate an increased therapeutic effect for mice treated with the G2/PAH-Cit/SeNPs@siRNA delivery system (Fig.10E).

Since the intra-tumoral VEGF content was associated with neovascularization, we then analyzed the microvessel density in tumors by using CD31 antibody (red fluorescence) and the nuclear counter-stain, DAPI (blue fluorescence).[10] As shown in Fig.10F, we observed a dramatically decreased microvessel density within the tumors treated with G2/PAH-Cit/SeNPs@siRNA, indicating a significant inhibition of tumoral vascularization. In comparison, SeNPs@siRNA treatment had a moderate effect. Thus, the G2/PAH-Cit/SeNPs@siRNA delivery system not only mediates a more efficient genetic silencing in tumor cells, but is also more suitable as a siRNA delivery system for *in vivo* cancer treatment.

The major organs (e.g. heart, liver, spleen, lung and kidney) of mice were also immediately harvested, fixed, and stained with hematoxylin and eosin (H&E) (Fig.S5). Compared to tissue from control mice (PBS treated), no significant mutative morphology or supersession of the viscera tissue were observed in mice following injection of either SeNPs@siRNA or G2/PAH-Cit/SeNPs@siRNA. We further quantified the selenium (Se) concentrations in main organs, including the heart, liver, spleen, lung, kidney, and tumor using, inductively coupled plasma mass spectrometry (ICP-AES). Fig.S6 shows that significantly more Se accumulation was seen in the tumors derived from SeNPs@siRNA and G2/PAH-Cit/SeNPs@siRNA delivery system-treated mice than in their major organs. These data confirm that G2/PAH-Cit/SeNPs@siRNA is able to selectively target the tumor, efficiently decrease blood vessels amount, and kill off tumor cells without lesions to major organs.

Conclusions

In summary, we have established that two pH-sensitive delivery systems, SeNPs@siRNA and G2/PAH-Cit/SeNPs@siRNA, can be loaded with VEGF siRNA and used to suppress VEGF gene expression both *in vitro* and *in vivo*. Additionally, the charge reversion delivery system G2/PAH-Cit/SeNPs had stronger binding affinities to the siRNA and greater release efficiency than SeNPs. The results of *in vivo* experiments showed that the

new G2/PAH-Cit/SeNPs@siRNA system significantly enhanced the anti-tumor effect on tumor-bearing mice, as indicated by *in vivo* VEGF gene silencing and reduced angiogenesis in tumors when compared to SeNPs@siRNA-treated mice. Detailed histological analysis revealed no lesions in major target organs. These obvious advantages could be attributed to the pH-response polymer PAH-Cit improve gene target releasing, and G2 PAMAM improve the loading efficiency of G2/PAH-Cit/SeNPs. These results indicate that our novel nanoparticle delivery system, G2/PAH-Cit/SeNPs@siRNA, has great potential to be used for *in vivo* therapeutic applications.

Aknowledgments

This work was supported by the National Natural Science Foundation of China (21171070, 21371075), the Planned Item of Science and Technology of Guangdong Province (c1211220800571), and the Fundamental Research Funds for the Central Universities.

Notes and references

[a]*Department of Chemistry, Jinan University, Guangzhou 510632, China*
[b]*Department ABCT, The Hong Kong Polytechnic University, Hong Kong*

**Corresponding authors. Department of Chemistry, Jinan University, Guangzhou 510632, China; Tel.: +86 20 85220223; fax: +86 20 85220223.E-mail addresses: tliuliu@jnu.edu.cn (J. Liu)*

[1]*Both authors contribute equally to this work*

†Electronic Supplementary Information (ESI) available: [details of any supplementary information available should be included here]. See DOI: 10.1039/b000000x

Reference

1 H. Arima, S. Yamashita, Y. Mori, Y. Hayashi, K. Motoyama, K. Hattori, T. Takeuchi, H. Jono, Y. Ando and F. Hirayama, *J. Control. Release*, 2010, **146**, 106-117.
2 D. N. Nguyen, J. J. Green, J. M. Chan, R. Langer and D. G. Anderson, *Adv. Mater*, 2009, **21**, 847-867.
3 K. A. Whitehead, R. Langer and D. G. Anderson, *Nat. Rev. Drug. Discov*, 2009, **8**, 129-138.
4 Y.-K. Oh and T. G. Park, *Adv. Drug. Deliv. Rev*, 2009, **61**, 850-862.
5 A. de Fougerolles, H.-P. Vornlocher, J. Maraganore and J. Lieberman, *Nat. Rev. Drug. Discov*, 2007, **6**, 443-453.
6 S. Tan, X. Li, Y. Guo and Z. Zhang, *Nanoscale*, 2013, **5**, 860-872.
7 Y. Zhang, J. M. Pelet, D. A. Heller, Y. Dong, D. Chen, Z. Gu, B. J. Joseph, J. Wallas and D. G. Anderson, *Adv. Mater*, 2013, **25**, 4641-4645.
8 A. C. Misra, S. Bhaskar, N. Clay and J. Lahann, *Adv. Mater*, 2012, **24**, 3850-3856.
9 N. Ferrara and R. S. Kerbel, *Nature*, 2005, **438**, 967-974.
10 P. N. Plummer, R. Freeman, R. J. Taft, J. Vider, M. Sax, B. A. Umer, D. Gao, C. Johns, J. S. Mattick and S. D. Wilton, *Cancer Res*, 2013, **73**, 341-352.
11 N. Ferrara, K. J. Hillan, H.-P. Gerber and W. Novotny, *Nat. Rev. Drug. Discov*, 2004, **3**, 391-400.
12 H.-Y. Wang, W.-J. Yi, S.-Y. Qin, C. Li, R.-X. Zhuo and X.-Z. Zhang, *Biomaterials*, 2012, **33**, 8685-8694.
13 X. Li, Y. Chen, M. Wang, Y. Ma, W. Xia and H. Gu, *Biomaterials*, 2013, **34**, 1391-1401.
14 C. A. Hong, J. S. Kim, S. H. Lee, W. H. Kong, T. G. Park, H. Mok and Y. S. Nam, *Adv. Funct. Mater*, 2013, **23**, 316-322.
15 D. Lin, Q. Cheng, Q. Jiang, Y. Huang, Z. Yang, S. Han, Y. Zhao, S. Guo, Z. Liang and A. Dong, *Nanoscale*, 2013, **5**, 4291-4301.
16 A. Nishiguchi, H. Yoshida, M. Matsusaki and M. Akashi, *Adv. Mater*, 2011, **23**, 3506-3510.
17 H. Liu, H. Wang, W. Yang and Y. Cheng, *J. Am. Chem. Soc*, 2012, **134**, 17680-17687.
18 X. Yang, X. Liu, Z. Liu, F. Pu, J. Ren and X. Qu, *Adv.Mater*, 2012, **24**, 2890-2895.
19 Y. Cheng, L. Zhao, Y. Li and T. Xu, *Chem. Soc. Rev*, 2011, **40**, 2673-2703.
20 J. L. Santos, H. Oliveira, D. Pandita, J. Rodrigues, A. P. P êgo, P. L. Granja and H. Tom ás, *J..Control.Release*, 2010, **144**, 55-64.
21 K. Luo, C. Li, L. Li, W. She, G. Wang and Z. Gu, *Biomaterials*, 2012, **33**, 4917-4927.
22 D. Chandrasekar, R. Sistla, F. J. Ahmad, R. K. Khar and P. V. Diwan, *Biomaterials*, 2007, **28**, 504-512.
23 J. Zong, X. Yang, A. Trinchi, S. Hardin, I. Cole, Y. Zhu, C. Li, T. Muster and G. Wei, *Nanoscale*, 2013, **5**, 11200-11206.
24 J. Zhang, X. Wang and T. Xu, *Toxicol. sci*, 2008, **101**, 22-31.
25 D. Sun, Y. Liu, Q. Yu, X. Qin, L. Yang, Y. Zhou, L. Chen and J. Liu, *Biomaterials*, 2014, **35**, 1572-1583.
26 D. Sun, Y. Liu, Q. Yu, Y. Zhou, R. Zhang, X. Chen, A. Hong and J. Liu, *Biomaterials*, 2013, **34**, 171-180.
27 J. Liu, Y. Huang, A. Kumar, A. Tan, S. Jin, A. Mozhi and X.-J. Liang, *Biotechnol. Adv*, 2013.

28 X. Liu, J. Zhang and D. M. Lynn, *Soft Matter*, 2008, **4**, 1688-1695.
29 Q. Li, T. Chen, F. Yang, J. Liu and W. Zheng, *Mater. Letters*, 2010, **64**, 614-617.
30 L. Han, J. Zhao, X. Zhang, W. Cao, X. Hu, G. Zou, X. Duan and X.-J. Liang, *ACS nano*, 2012, **6**, 7340-7351.
31 Q. Yu, Y. Liu, C. Wang, D. Sun, X. Yang, Y. Liu and J. Liu, *PloS one*, 2012, **7**, e50902.
32 S. Guo, Y. Huang, Q. Jiang, Y. Sun, L. Deng, Z. Liang, Q. Du, J. Xing, Y. Zhao and P. C. Wang, *Acs Nano*, 2010, **4**, 5505-5511.
33 Y. F. Tan, R. C. Mundargi, M. H. A. Chen, J. L. essig, B. Neu, S. S. Venkatraman, T. T. Wong, *Small*, 2014, DOI: 10.1002/smll.201303201
34 Z. J. Deng, S. W. Morton, E. Ben-Akiva, E. C. Dreaden, K. E. Shopsowitz, P. T. Hammond, *ACS nano*, 2013, **7**, 9571-9584.
35 R. Esfand and D. A. Tomalia, *Drug. Discov. Today*, 2001, **6**, 427-436.
36 S. Guo, Y. Huang, , Q. Jiang, Y. Sun, L. Deng, Z. Liang, Q. Du, J. Xing, Y. Zhao, P. C. Wang, ACS Nano, 2010, 4, 5505-5511.
37 H. Liu, H. Wang, W. Yang, Y. Cheng, J. Am. Chem. Soc, 2012, 134, 17680− 17687
38 N. Ferrara, H.-P. Gerber and J. LeCouter, *Nat. Med*, 2003, **9**, 669-676.
39 S. Bhargava, B. Hotz, O.J. Hines, , H.A. Reber, H.J. Buhr, H.G. Hotz, *J. Gastrointest. Surg*, 2007, **11**, 171-178.
40 A. Gagliardi, H. Hadd, D. Collins, *Cancer. Res*, 1992, **52**, 5073-5075.
41 D. Marino, Y. Angehrn, S. Klein, S. Riccardi, N. Baenziger-Tobler, V. I. Otto, M. Pittelkow and M. Detmar, *J. Dermatol. Sci*, 2013, **71**, 184-194.
42 S. K. Lee and C. H. Tung, *Adv. Funct. Mater*, 2013, **23**, 3488-3493.
43 H. Chen, B. Li, J. Qiu, J. Li, J. Jin, S. Dai, Y. Ma and Y. Gu, *Nanoscale*, 2013, **5**, 12409-12424.